Distinct denitrification phenotypes in closely related bacteria: clues to understanding variations in nitrite accumulation among *Stutzerimonas* strains

Martin Menestreau[1], Daniel A. Milligan[1], Louise B. Sennett[1], Linda Bergaust[1], Lars R. Bakken[1], Gary Rowley[2], Morten Kjos[1], James P. Shapleigh[3] and Åsa Frostegård[1]

[1] Faculty of Chemistry, Biotechnology, and Food Sciences, Norwegian University of Life Sciences, Norwegian University of Life Sciences, Ås, Norway

[2] School of Biological Sciences, University of East Anglia, Norwich, United Kingdom

[3] Department of Microbiology, Cornell University, Ithaca, NY, USA

Correspondance: Åsa Frostegård (asa.frostegard@nmbu.no)

Funding: This work was supported by the Research Council of Norway, project no. 325770 (awarded to Å.F.).

Running title: Nitrite accumulation in *Stutzerimonas* strains

Keywords: Denitrification phenotypes, Nitrite accumulation, *Stutzerimonas* strains

Author details:

Martin Menestreau, e-mail: martin.menestreau@nmbu.no; ORCID id: 0000-0001-5060-5903

Daniel A. Milligan, e-mail: daniel.a.milligan@gmail.com; ORCID id: 0009-0002-3792-1308

Louise B. Sennett, e-mail : louise.sennett@nmbu.no; ORCID id: 0000-0001-5445-9712

Linda Bergaust, e-mail: linda.bergaust@nmbu.no; ORCID id: 0000-0001-5100-6611

Lars R. Bakken, e-mail: lars.bakken@nmbu.no; ORCID id: 0000-0002-7293-8108

Gary Rowley, e-mail: g.rowley@uea.ac.uk; ORCID id: 0000-0002-5421-4333

Morten Kjos, e-mail: morten.kjos@nmbu.no; ORCID id: 0000-0003-4448-9082

James P. Shapleigh, e-mail: jps2@cornell.edu; ORCID id: 0000-0002-8628-3966

Åsa Frostegård, e-mail: asa.frostegard@nmbu.no; ORCID id: 0000-0002-4754-5994

Abstract

Nitrite (NO_2^-) is a key denitrification intermediate, formed from nitrate (NO_3^-). Transient NO_2^- accumulation varies among denitrifiers, yet the underlying causes remain poorly understood, despite its potential toxicity and role in NO and N_2O emissions. We profiled eighteen related *Stutzerimonas* strains, including the model *S. perfectomarina* ZoBell, and identified three phenotypic clusters (full, partial and low nitrite accumulators; FNA, PNA and LNA) based on the fraction of NO_3^--N transiently accumulated as NO_2^-. LNA strains lack or express the membrane-bound nitrate reductase (NarG) late, relying on periplasmic NapA for NO_3^- reduction, possibly explaining their balanced NO_2^- production/reduction. FNA and PNA strains possess NapA and NarG but differ in their nitrite reductase (NirS) clades. Delayed *nirS* transcription as FNA strains transition to NO_3^- respiration likely accounts for some NO_2^- accumulation. However, addition of NO_3^- halted NO_2^- reduction in FNA strains, suggesting additional metabolic control. This may require the cytochromes NirTB, which are only found in FNA strains. The regulator DnrE was also unique to NO_2^--accumulators, likely having a role in finetuning NO_2^- regulation. Our findings reveal diverse NO_2^--handling phenotypes among denitrifiers and provide insights for optimizing wastewater nitrogen removal and soil bioaugmentation strategies to mitigate N_2O emissions.

Introduction

Denitrification is one of the main pathways driving the global nitrogen cycle. Complete denitrification is the four-step reduction of nitrate (NO_3^-) to dinitrogen (N_2) via the intermediate products nitrite (NO_2^-), nitric oxide (NO) and nitrous oxide (N_2O). In this process, the denitrification enzymes Nar, Nir, Nor and Nos are responsible for reduction of NO_3^-, NO_2^-, NO and N_2O, respectively (Berks et al. 1995; Zumft 1997). A wide variety of facultative anaerobic organisms, including bacteria, archaea and fungi, can perform all or some of the reduction steps associated with denitrification (Shapleigh 2013; Roothans et al. 2025). A shared trait amongst all denitrifiers is that O_2 is the preferred electron acceptor, but if the O_2 concentration decreases, denitrifiers use a variety of regulatory mechanisms to switch from O_2 to N-oxides as electron acceptors (Spiro 2007; Bakken et al. 2012), leading to large variations in their transient accumulation of denitrification

55 intermediates (Lycus et al. 2017). Current knowledge of how denitrifiers control the transition from aerobic
56 respiration to denitrification is largely based on studies of a few model organisms capable of complete
57 denitrification of NO_3^- to N_2. These studies have resulted in a relatively clear, though likely incomplete,
58 understanding of transcriptional and post-transcriptional mechanisms influencing denitrification
59 phenotypes (Spiro, 2012; Vaccaro et al. 2016; Gaimster et al. 2018).

60 One knowledge gap is the understanding of mechanisms controlling NO_2^- accumulation in
61 denitrifying bacteria (Liu et al. 2013). Nitrite is a central molecule in the nitrogen cycle that can be produced
62 and consumed in many redox processes, and its reduction is the defining reaction of denitrification (Kuypers
63 et al. 2018). In its protonated form, HNO_2, it can diffuse into cells and cause damage itself or through the
64 formation of toxic, reactive nitrogen species (Chislett et al. 2022). Moreover, accumulation of NO_2^- in the
65 environment can cause increased emissions of the greenhouse gas N_2O by impairing N_2O reduction
66 (Highton et al. 2022) or by producing N_2O through reactions with ferrous iron or organic matter compounds
67 (Van Cleemput and Samater 1995). Paradoxically, in some systems, NO_2^- accumulation is desirable. One
68 example is denitratation in wastewater treatment plants, where denitrification is used instead of ammonia
69 oxidation to provide nitrite for the anammox process (Zhuang et al. 2022).

70 The best-studied denitrifying bacteria, *Paracoccus denitrificans*, *Pseudomonas aeruginosa* and
71 *Pseudomonas stutzeri* ZoBell, all transiently accumulate some NO_2^- during anaerobic growth on NO_3^-
72 (Carlson and Ingraham 1983). However, studies extending beyond these model organisms have revealed
73 substantial variations in NO_2^- accumulation among diverse taxa (Lycus et al. 2017). A comparison of
74 *Thauera* strains (Liu et al. 2013) showed that some exhibited a rapid and complete onset (RPO) of all four
75 steps of the denitrification pathway, resulting in little to no NO_2^- accumulation. Others displayed a
76 progressive onset (PO) in which all available NO_3^- was reduced to NO_2^- prior to any reduction of NO_2^- took
77 place, leading to NO_2^- accumulation. A shared feature of the RPO strains was that they carried the
78 periplasmic NapA for dissimilatory NO_3^- reduction but lacked the membrane-bound NarG, while the PO
79 strains carried both NapA and NarG. All strains induced NO_3^- reduction as O_2 approached depletion, but

80 the regulatory dynamics varied. In the RPO strains, transcription of the *nirS* and *nosZ* genes - which encode
81 Nir and Nos, respectively – was initiated concurrently with Nar. In contrast, the NO_2^- accumulating PO
82 strains delayed transcription of these genes until all available NO_3^- had been reduced to NO_2^-. This led to
83 the tentative suggestion that a NO_3^- responsive mechanism might regulate *nir*-transcription in the NO_2^-
84 accumulating strains, although no direct evidence for this was found (Liu et al. 2013).

85 The present study was initiated to clarify how regulatory mechanisms drive variations in
86 denitrification phenotypes, and how these can differ even among closely related bacteria, with a particular
87 focus on NO_2^- accumulation. We compared eighteen strains within the former *Pseudomonas stutzeri* species
88 cluster, now reclassified as the genus *Stutzerimonas* (Lalucat et al. 2022). This complex contains
89 metabolically versatile organisms that are widespread in various environments (Lalucat et al. 2006). We
90 combined genome analyses with determinations of high-resolution denitrification kinetics and transcription
91 patterns of denitrification related genes during and after transition from aerobic to anaerobic respiration.
92 Using deletion mutations, we investigated whether the Crp/Fnr-like regulator DnrE, known to affect
93 transcriptional regulation in *S. stutzeri* (Härtig et al. 1999), influences NO_2^- accumulation in a closely related
94 strain. Moreover, we explored the potential role of sRNAs, which can act as both activators and repressors
95 of transcription and translation and have been shown to influence denitrification via control of NirR in *P.*
96 *denitrificans* (Gaimster et al. 2018; Moeller et al. 2021). We also considered whether electron competition
97 between electron pathways to the different denitrification reductases (Cole 2025; Richardson 2025) could
98 explain differences in NO_2^- accumulation among the *Stutzerimonas* strains. Electrons are delivered from
99 the TCA cycle via dehydrogenases, such as NADH or FDH dehydrogenase, to the quinone/quinol pool,
100 which serves as a key branching point in the electron transport chain. In complete denitrifiers, electrons are
101 then directed either to NO_3^- reductases (NapA, NarG) or to the bc_1 complex, a second branching point, from
102 which electrons are passed to Nir, Nor, and NosZ via cytochromes or azurins/pseudoazurins. Competition
103 occurs primarily at these branching points (Chen and Strous, 2013; Mania et al. 2020). In this study, we
104 specifically investigated the electron competition between NO_3^- and NO_2^- reduction pathways.

105 Our results categorize the eighteen strains into three distinct phenotypic groups showing full, partial
106 or low NO_2^- accumulation (FNA, PNA and LNA). A major difference among these phenotypes was the
107 presence and regulation of dissimilatory NO_3^- reductases (Nar/Nap), with Nar either absent or showing
108 delayed transcription in LNA strains. Among the NO_2^--accumulating strains (FNA and PNA), differences
109 were associated with *nir* gene cluster arrangement and NirS clade affiliation. Additional differences among
110 phenotypic groups were observed in the transcriptional patterns of denitrification reductase genes and in
111 the metabolic control of NO_3^- and NO_2^- reduction pathways. These findings indicate that denitrification
112 phenotypes cannot be predicted solely from gene content but are instead governed by a multilayered
113 regulatory network operating at both transcriptional and post-transcriptional levels. Since NO_2^- is a central
114 molecule in the biochemical N-cycle and is utilized by several biological processes, this knowledge is
115 important for developing biotechnological approaches, such as using denitrifiers in combination with
116 anammox bacteria for improved wastewater treatment technologies, or engineering the soil microbiome in
117 agriculture to reduce greenhouse gas emissions.

118

119 # Materials and Methods

120 ## Strains and growth conditions

121 Eighteen bacterial strains, previously classified as belonging to the *P. stutzeri* species complex (Lalucat et
122 al. 2006; Li et al. 2022), were selected for comparison of their denitrification phenotypes. The strains were
123 obtained from various culture collections. A recent taxonomic revision of the genus *Pseudomonas*
124 reclassified these strains into several species of the novel genus *Stutzerimonas* (Lalucat et al. 2022; Gomila
125 et al. 2022). A list of the strains, including their origin of isolation and culture collection accession numbers,
126 is found in Table S1.

127 All strains were incubated at 20°C in 120 mL serum vials containing 50 mL Sistrom's mineral
128 medium (Sistrom 1960; Bergaust et al. 2010) supplemented with 2 mM KNO_3 or KNO_2, added as filter
129 sterilized solutions. Vials prepared for cultivation under limited O_2 conditions were sealed with gas tight

130 butyl rubber septa and aluminum caps (Matriks AS, Norway), and air was evacuated from the 70 mL
131 headspace by six repetitions of applying vacuum for 360 s and He overpressure for 30 s. The overpressure
132 was released prior to the injection of the desired amount of O_2 and N_2O. Near-equilibrium between
133 headspace and the liquid phase was maintained by vigorous stirring at 600 rpm using a Teflon-coated
134 triangular magnetic bar. The stirring also prevented cell aggregation, ensuring that the cells were evenly
135 dispersed and experienced the intended gas concentrations. At the start of each experiment, the vials were
136 inoculated with 1 mL of aerobically growing bacterial cultures to an initial OD_{600} of 0.05-0.10. The cultures
137 had been raised from frozen stocks and pre-cultured with vigorous stirring under fully oxic conditions for
138 at least 4 generations to minimize the amounts of previously synthesized denitrification enzymes in the
139 cells (Mania et al. 2020; Gao et al. 2021).

140 Gas kinetics and chemical analyses

141 Headspace gases were monitored using a robotized incubation system as described in Molstad et al. (2007)
142 and Molstad et al. (2016). Briefly, gas samples were taken automatically by an autosampler (Agilent GC
143 Sampler 80) through the rubber septa of the vials using a peristaltic pump. The samples were then pumped
144 into a gas chromatograph (Agilent 7890A) for analysis of O_2, N_2O, N_2 and CO_2 and into a
145 chemifluorescence NO analyzer (Model 200A, Advanced Pollution Instrumentation). A thermal
146 conductivity detector was used to measure O_2 and N_2, while an electron capture detector was used to
147 measure N_2O. To maintain a slight overpressure in the vials, each 1 mL gas sample was replaced with a
148 slightly larger volume of He at near-atmospheric pressure. Three replicate vials were measured for each
149 treatment unless otherwise stated (n=3).

150 To determine NO_2^- concentrations, samples were collected from a parallel set of vials to avoid
151 sampling losses and changes in the headspace-to-liquid ratio. The samples were collected manually at
152 regular intervals through the rubber septum using a sterile syringe. Concentrations of NO_2^- were determined
153 immediately after each sampling, using the methodology described in Lim et al. (2018), which is based on
154 the method by Braman and Hendric (1989) and Cox (1980). Briefly, 10 µl liquid sample was injected into

155 a purging device containing a reducing agent (NaI) in 50% acetic acid at room temperature and the NO
156 produced was measured with a chemifluorescence NOx analyzer (Sievers NOA 280i). Samples from three
157 replicate vials were measured (n=3). Calculations based on cubic spline interpolation allowed estimation
158 of values between sampling times.

159 Statistical analyses

160 Statistical analyses were performed using the base statistics software in RStudio. In brief, one-way analysis
161 of variance (ANOVA) tests were performed to assess whether there were significant differences in the
162 levels of denitrification intermediates produced by the different NO_2^- accumulation phenotypes and by the
163 various overexpression mutants. When differences occurred ($p = 0.05$), mean pairwise comparisons were
164 performed using Tukey's test (HSD) for the post hoc analysis of the ANOVA models. Normality was tested
165 using homoscedasticity plots and the Shapiro-Wilks test of the residuals ($p > 0.05$).

166 Transcription analysis

167 Samples for RNA extraction (approximately 5 x 10^8 cells per sample) were taken at intervals from the liquid
168 phase. Cells were pelleted at 10,000 g for 7 minutes at 4°C and stabilized using RNAprotect (Bacteria
169 Reagent, Qiagen) according to the manufacturer's protocol. Total RNA was extracted using the RNeasy
170 Mini Kit (Quiagen). RNA concentrations were measured using the Qubit RNA BR Assay Kit (Life
171 Technologies). Genomic DNA was removed with Turbo DNase (Life Technologies) and genomic DNA
172 contamination was ruled out by SYBR green qPCR amplification using primers for *nosZ* (Table S2) prior
173 to reverse transcription. The assays were run on an Applied Biosystems StepOnePlus system, and samples
174 with values < 5 *nosZ* copies per reaction were deemed gDNA free (Lim et al. 2016). Reverse transcription
175 was then carried out with Maxima First Strand cDNA Synthesis Kit (Thermo Scientific), the product was
176 diluted, and gene transcripts were quantified by digital droplet PCR (ddPCR). A ddPCR reaction mix was
177 prepared (QX200 ddPCR EvaGreen supermix; Bio-Rad). Oil droplet suspensions were prepared using a
178 QX200 droplet generator (Bio-Rad), and PCR reactions were performed using the temperature program:
179 enzyme activation at 95 °C for 5 min; 40 cycles of denaturation at 95 °C for 30 s and combined

180 annealing/extension at 60 °C for 1 min; followed by signal stabilization at 4 °C for 5 min and a final step
181 at 90 °C for 5 min. PCR products were quantified using a QX200 droplet reader (Bio-Rad) and the data was
182 analyzed using QuantaSoft Analysis Pro 1.0.596 (Bio-Rad). All primers used are listed in Table S2.

183 Deletion of *narG* and *dnrE* in *Stutzerimonas decontaminans* strain 19SMN4

184 The pACRISPR/pCasPA system developed by Chen et al. (2018) for genome editing in various
185 *Pseudomonas* species was used to construct the two deletion mutants, Δ*narG* and Δ*dnrE*, in *Stutzerimonas*
186 *decontaminans* 19SMN4. pACRISPR plasmids specific to the targeted gene were constructed to contain a
187 spacer targeting the specific gene designed using the tool CRISPOR (Concordet and Haeussler 2018) and
188 a repair template consisting of 1000-bp flanking sequences, upstream and the downstream of the gene. The
189 pCasPA was electroporated into *S. decontaminans* strain 19SMN4 following the protocol of Choi et al.
190 (2006), but with electroporation parameters optimized for this strain (2500V, 200Ω, 25µF, 2 mm cuvette).
191 Colonies containing pCasPA were selected after incubation on LB agar in the presence of 50 µg mL^{-1}
192 tetracycline. Before the second electroporation for introduction of the gene specific plasmid pACRISPR,
193 the strain containing the pCasPA plasmid was induced for 2 hours with 2 mg mL^{-1} L-arabinose, followed
194 by electroporation under the same conditions as the first electroporation. Transformants were then selected
195 on 50 µg mL^{-1} tetracycline and 150 µg mL^{-1} carbenicillin plates. The deletions were validated by PCR (for
196 primers see Table S2) and Sanger sequencing. Colonies of successfully mutated cells were restreaked one
197 to three times on LB agar supplemented with 10% w/v sucrose to cure the plasmids from the cells.

198 *Stutzerimonas perfectomarina* ZoBell sRNA overexpression mutants

199 Small RNAs (sRNAs) were overexpressed in *Stutzerimonas perfectomarina* ZoBell using the arabinose-
200 inducible vector pL2020 (Sommer et al. 2017). The pL2020 plasmid was linearized by digestion with NdeI
201 and HindIII. sRNAs were amplified from *S. perfectomarina* ZoBell genomic DNA using overlapping PCR.
202 The resulting PCR fragments were assembled with the digested vector using the NEBuilder HiFi DNA
203 Assembly Master Mix (New England Biolabs) and transformed into *E. coli* DH5α competent cells.
204 Transformants were selected on LB agar plates containing 30 µg mL^{-1} chloramphenicol. Positive clones

205 were screened by colony PCR and verified by Sanger sequencing. Constructed plasmids were subsequently
206 electroporated into the *S. perfectomarina* ZoBell host strain using an adapted protocol (Choi et al. 2006)
207 with optimized electroporation parameters as described above. The growth of the sRNA overexpression
208 mutants was assessed in LB medium supplemented with 30 μg mL^{-1} chloramphenicol to maintain plasmid
209 selection.

210 Genome sequencing and assembly

211 DNA was extracted with the QIAmp DNA Mini Kit (Qiagen, USA) and sent to the Norwegian Sequencing
212 Centre (University of Oslo) for TruSeq Nano preparation and Illumina MiSeq sequencing. Reads were
213 trimmed using Nesoni clip (https://github.com/Victorian-Bioinformatics-Consortium/nesoni) and contigs
214 were assembled using Velvet (Zerbino and Birney 2008). Sequence annotation was carried out on the RAST
215 server (Aziz et al. 2008). NCBI accession numbers are listed in Table S1.

216 Gene sequence analyses and phylogenetic determinations

217 Sequences coding for housekeeping genes assigned to strains in the *P. stutzeri* species complex, as well as
218 regulatory and structural genes encoding relevant nitrogen cycle processes, were retrieved from the NCBI
219 databases. For protein-coding genes, the match sequences that represented uninterrupted open reading
220 frames (ORFs) were identified, and gene synteny was compared for strains for which extensive operon data
221 was available. The phylogenetic relationship of the strains was determined based on a multilocus sequence
222 analysis (MLSA) of the genes encoding the small subunit RNA (16S rRNA), gyrase B (*gyrB*) and RNA
223 polymerase (*rpoD*). The sequences were complete, except in the case of 16S rRNA genes where the first
224 30 residues were omitted, as they were not available for strain DSM 50238. Genes were aligned using
225 MUSCLE v. 3.8.31 (Edgar 2004) and examined before Jukes Cantor distance estimation and maximum-
226 likelihood tree construction, using PhyMl 3.1 (Guindon et al. 2010). Amino acid-based enzyme phylogenies
227 were calculated using Clustal Omega (Sievers et al. 2011) and phylogenetic trees were constructed using
228 the Whelan and Goldman model in PhyMl.

229 # Results

230 ## Nitrite accumulation phenotypes and phylogeny

231 Analyses of the denitrification phenotypes revealed significant differences in transient NO_2^- accumulation
232 among the strains (Table 1). When incubated under denitrifying conditions with initially 100 µmol vial^{-1} of
233 NO_3^- (2 mM), the full nitrite accumulator (FNA) strains reduced ≥89 % of the provided NO_3^- to NO_2^- before
234 any NO_2^- reduction took place (Figure 1a and Figure S1). The partial nitrite accumulator (PNA) strains
235 (Figure 1b and Figure S2) exhibited transient NO_2^- accumulation, amounting to about half of the provided
236 NO_3^- (43.7- 62.2 µmol vial^{-1} of NO_2^-). The low nitrite accumulator (LNA) phenotype (Figure 1c and Figure
237 S3) showed no or little NO_2^- accumulation (0.2-1.6 µmol vial^{-1}), except for strains 24a75 and 4C29, which
238 transiently accumulated 11.3 and 17.1 µmol NO_2^- vial^{-1}, respectively.

239 A phylogenetic tree was constructed, incorporating the eighteen *Stutzerimonas* strains selected for
240 analysis of denitrification phenotypes, along with additional related strains. Each strain´s classification is
241 marked in the phylogenetic tree with red (FNA), yellow (PNA) or blue (LNA) (Figure 2). The tree was
242 based on multilocus sequence analysis (MLSA) of two complete housekeeping genes (*gyrB* and *rpoD*) and
243 nearly complete 16S rRNA gene sequences. Only limited congruence was observed between phylogeny
244 and the NO_2^- accumulation phenotype: FNA and PNA strains clustered together and were often intertwined,
245 whereas LNA strains were distributed across multiple, widely separated branches. The neighbor joining
246 tree based on kmer clustering of a more extensive collection of genomes from *Stutzerimonas* strains (Figure
247 S4) revealed a similar pattern, also consistent with other recently published phylogenetic studies (Li et al.
248 2022; Gomila et al. 2022).

249 ## Selected genetic features related to denitrification

250 An analysis of denitrification related gene clusters was performed to identify possible relationships with
251 the NO_2^- accumulation phenotypes (Table 1). All eighteen strains had genetic potential to perform complete
252 denitrification. They all carry the *napEDABC* gene cluster encoding periplasmic nitrate reductase (Nap).
253 Nap also was the dominant NO_3^- reductase in the clustered set of genomes (Figure S4). Two strains in the
254 LNA group (DNSP21 and 28a3) rely only on Nap for dissimilatory NO_3^- reduction, since they lack the

255 cytoplasmic nitrate reductase Nar, encoded by the *nar* genes. The *narGHJIKMXL* cluster was found in all
256 other strains. A notable difference in *nar*-related genes among the phenotype groups was the presence of
257 the *dnrE* gene, which was found in all FNA and PNA strains but was absent in all LNA strains. DnrE is
258 located within the *nar* gene cluster. It belongs to the group dissimilatory nitrate respiration regulators
259 (DNR), a subgroup of transcriptional regulators related to the Fnr/Crp family (Trunk et al. 2010; Ebert et
260 al. 2017), and has a potential role in regulating the *narG* gene expression (Härtig et al. 1999).

261 All analyzed strains carried the *nirS* gene encoding the cytochrome cd_1 nitrite reductase (Zumft
262 1997). The *nirS* gene is part of a large gene cluster encoding various enzymes involved in the synthesis and
263 function of NirS (Jüngst et al. 1991; Philippot 2002). The FNA and PNA strains have identical *nirS* gene
264 cluster configurations, apart from the presence of *nirTB* in the FNA strains, while the *nirS* gene cluster in
265 the LNA strains is more diverse (Figure S5). Based on their amino acid sequences, the NirS reductases
266 have been divided into several clades. (Jones et al. 2008; Pold et al. 2024). Following this classification,
267 the NirS type of the FNA organisms in the present study belongs to clade 1b, while that of the PNA and
268 LNA strains belong to clade 1a (Table 1), except the LNA strain JM300 which carries the NirS clade 1b
269 (Figure S5). A common trait for all analyzed (Table 1) or clustered (Figure S4) *Stutzerimonas* strains with
270 clade 1b NirS is the consistent presence of the genes *nirT* and *nirB*. NirT and NirB are tetraheme and diheme
271 cytochromes, respectively, with a putative role in electron transfer and possibly also in the catalytic
272 activation of the cd_1 cytochrome (Härtig and Zumft 1999; Zajicek et al. 2004). The *nirTB* genes are absent
273 in all clade 1a strains.

274 Of the 314 genomes in the clustered tree (Figure S4), 111 carried the *nirK* gene, which encodes the
275 copper-containing nitrite reductase NirK. Among the analyzed strains, seven possessed both *nirK* and *nirS*
276 (Table 1). Notably, *nirK* was present in strains across all three NO_2^- accumulator groups. Previously, *nirK*
277 was divided into two main clades based on copper-binding histidine motifs: TRPHL for clade I; and
278 SSFH(V/I/P) for clade II (Jones et al. 2008; Declayre et al. 2016). A recent study (Pold et al. 2024) proposed
279 a more detailed classification, reassigning *Stutzerimonas* strains with clade I NirK to clade 1a, and those

280 with clade II to clade 1e. In the analyzed *Stutzerimonas* strains carrying the *nirK* clade I gene (1a), the gene
281 is consistently followed by *nirV*. This was observed in two of the strains in the present study, both belonging
282 to the LNA phenotype group (Table 1). Half of the FNA strains analyzed in this study, along with one PNA
283 strain, possess *nirK* clade II (1e), consistently followed by the *norCBQD* gene cluster.

284 The nitric oxide reductase cNor, which was present in all eighteen strains, is encoded by the
285 *norCBD* operon located in the denitrification island together with the *nir* and *nos* clusters (Zumft 1997;
286 Vollack et al. 1998). The *norCBQD* cluster present downstream of the *nirK* clade II gene in some of the
287 FNA and PNA strains may be used under conditions when *nirK* is expressed, given their proximity. The
288 gene cluster *nosRZDFYL* encoding the nitrous oxide reductase (NosZ) clade I was also found in the
289 denitrification island in all the studied *Stutzerimonas* strains. The *nor* and *nos* gene cluster arrangements
290 were identical in all strains (Table 1).

291 Denitrification kinetics and transcription analysis

292 Electron flow rates to the different reductases were calculated from denitrification kinetics measured for all
293 eighteen strains during and after the switch from aerobic respiration to denitrification when incubated with
294 1% initial O_2 and 2 mM NO_3^- (100 µmol vial^{-1}). All strains could perform the complete denitrification
295 process, reducing NO_3^- to N_2. Examples for some representative strains are shown in Figures 1 and 3, while
296 Figures S1, S2 and S3 show the denitrification kinetics for the remainder. Common to all strains,
297 irrespective of which NO_2^- accumulation group they belonged to, was that NO_3^- reduction started when the
298 O_2 had decreased to 10-15 µmol vial^{-1} (corresponding to 0.6-0.9 µM in the liquid). The FNA strains reduced
299 all the provided NO_3^- to NO_2^- before any NO_2^- reduction took place, as shown by the lack of intermediate
300 gas products (Figure 1a and Figure S1). The start of NO_2^- reduction coincided with the peak of NO_2^-
301 accumulation and was accompanied by nearly simultaneous production of NO, N_2O and N_2. The sequential
302 reduction of NO_3^- and NO_2^- in the FNA strains is also reflected in the electron flow kinetics (Figure 1d and
303 Figure S1), with nearly no overlap between the curve showing the electron flow rate to NO_3^- ($V_{eNar/Nap}$, red
304 shading) and that to NO_2^- (V_{eNir}; purple shading) and a clear separation between O_2 reduction (V_{eO2}; blue

305 shading) and NO_2^- reduction (V_{eNir}; purple shading). The electron flow for the FNA strains typically showed
306 a prominent dip when the cultures shifted from NO_3^- reduction to NO_2^- reduction (Figure 1d, Figure 3e and
307 Figure S2), suggesting that only a fraction of the cells respired NO_2^- as found for *Paracoccus denitrificans*
308 (Lycus et al. 2018).

309 The PNA and LNA strains reduced NO_3^- and NO_2^- simultaneously, as indicated by the production
310 of NO and N_2O, followed by the appearance of N_2 (Figure 1b-c, Figure S2 and Figure S3). The strains
311 CCUG 11256 (PNA) and 28a3 (LNA) were similar in their denitrification phenotypes (Figure 1b-c), except
312 for the transient accumulation of NO_2^- by the PNA strain. The simultaneous reduction of NO_3^- and NO_2^-
313 was reflected in the overlap between the areas under the curves for $V_{eNar/Nap}$ (red shading) and V_{eNir} (purple
314 shading) (Figure 2e-f, Figure S2 and Figure S3). Production of N_2 was detected somewhat later, when O_2
315 was near depletion. For both the PNA and LNA groups, the electron flow indicated smooth transitions
316 between the different electron acceptors with no distinct dips and thus an overlap between the curves for
317 $V_{eNar/Nap}$ and Ve_{Nir}.

318 All three NO_2^- accumulation phenotypes showed little transient accumulation of NO and N_2O
319 (Table 1), suggesting a strong regulatory control of the production and consumption of these gaseous
320 denitrification intermediates. When incubated with 1% initial O_2 and 2 mM initial concentration of NO_3^-,
321 the maximum net NO production was 9.1–70.5 nmol vial^{-1} with no significant (p = 0.598) difference
322 between the phenotype groups in terms of maximum NO accumulation. The N_2O accumulation remained
323 low for all strains, ranging between 0.3 and 89 nmol vial^{-1}, and was significantly lower for FNA compared
324 to LNA (p = 0.030), while PNA exhibited intermediate levels, showing no significant difference from either
325 FNA or LNA (p = 0.840 and 0.217).

326 Transcription of the denitrification reductase genes *narG, napA*, *nirS*, *norB* and *nosZ* was monitored
327 in the strains ZoBell (FNA) and JM300 (LNA) during and after the transition from aerobic respiration to
328 denitrification, along with the denitrification kinetics (Figure 3). In addition, transcription of the *nirK* gene,
329 which is lacking in strain ZoBell (Table 1), was monitored in strain JM300. Strain ZoBell reduced all NO_3^-

330 (100 µmol vial^{-1}) to NO_2^- before any significant NO_2^- reduction took place (Figure 3a), confirming its
331 classification into the FNA group. This was also reflected in the electron flow kinetics which showed that
332 electrons were channeled to Nir only once the electron flow to Nar stalled due to NO_3^- depletion (Figure
333 3e). Transcription of *napA* and *nosZ* in strain ZoBell (Figure 3c) was detected already at 0 hpi (hours post
334 inoculation). Increased transcription was observed for all the monitored genes at 10-13 hpi when less than
335 10 µmol of O_2 remained in the vial, with an initial transcription peak for most genes at 18 hpi. Although
336 transcripts for genes involved in all four denitrification steps were detected during this initial peak, it
337 resulted in only minimal reduction activity, except for NO_3^- reduction. A second pulse of transcription
338 occurred once all NO_3^- had been reduced and the NO_2^- concentration reached its maximum. During this
339 second event, the maximal levels of *norB* and *nirS* (inset) transcription were observed at 30-35 hpi. There
340 was also a notable increase in *nosZ* transcription, although not surpassing what was measured in the initial
341 phase. These peaks corresponded to the nearly simultaneous reduction of NO_2^-, NO and N_2O (Figure 3a).
342 Transcription was sustained until all intermediates were fully reduced to N_2.

343 The LNA strain JM300 (Figure 3b, d, f) reduced NO_3^- to gases, via NO_2^-, without any detectable
344 net accumulation of NO_2^-. NO and N_2O became detectable when the O_2 concentration was approximately
345 20 µmol vial^{-1}, corresponding to1.2 µM in the liquid (at 7.5 hpi), consistent with previous findings for this
346 strain (Wittorf et al. 2018). Concentrations of these gases peaked around 11 hpi, immediately followed by
347 N_2 production. The simultaneous reduction of the different electron acceptors is seen in the gradual increase
348 in total electron flow rates in JM300 as well as in the other LNA strains (Figure 3f and Figure S3). Also
349 notable is the absence of the significant dip in the electron flow rates that was observed in most of the FNA
350 strains during the shift from NO_3^- to NO_2^- reduction (Figure 3e and Figure S1). The overlapping $V_{eNar/Nap}$
351 and V_{eNir} curves (Figure 3f) reflect the simultaneous reduction of NO_3^- and NO_2^-, also observed for the other
352 strains characterized as LNA (Figure 2c, f and Figure S3). An important finding was that *narG* transcription
353 was delayed by five hours compared to the other genes, indicating that NO_3^- reduction was carried out by
354 the periplasmic nitrate reductase Nap during the early phase of denitrification. A slight delay in the
355 transcription of *nirS*, *nirK*, and *norB* was also observed compared to *napA* and *nosZ*. Like this LNA strain

356 (JM300), delayed *narG* transcription was seen in the LNA strain DSM 50238 (Figure S6), which exhibited
357 a transcriptional profile similar to JM300, although it lacks *nirK*.

358 Effect of *narG* and *dnrE* deletions on nitrite accumulation

359 The wild-type PNA strain 19SMN4 carries *narG*, which is either absent (Table 1) or transcribed with a
360 delay (Figure 3 and Figure S6) in the LNA strains, as well as *dnrE*, which is absent in all the LNA strains
361 (Table 1). We hypothesized that deletion of either gene would shift strain 19SMN4 from the PNA to the
362 LNA phenotype. Specifically, we predicted that NO_3^- reduction rate would slow down in the *narG* mutant,
363 as it would rely solely on the periplasmic NO_3^- reductase Nap for dissimilatory NO_3^- reduction, resulting in
364 decreased NO_2^- accumulation. Furthermore, given that all LNA strains lack the *dnrE* gene (Table 1), we
365 hypothesized that the absence of this transcriptional regulator would reduce or delay the transcription of
366 *narG* in the presence of NO_3^-, compared to the wild-type. This would similarly result in reduced NO_2^-
367 accumulation producing a phenotype resembling that of the LNA strains. To test these hypotheses, we
368 generated deletion *narG* and *dnrE* mutants in the PNA strain 19SMN4.

369 A comparison of the denitrification phenotypes of the wild-type and the two mutants showed that
370 the mutants remained complete denitrifiers, as all provided NO_3^- was fully reduced to N_2 (Figure 4). Both
371 the wild-type and the mutants transitioned to denitrification, indicated by the accumulation of low amounts
372 of NO (16.5-43.2 nmol vial^{-1}) and N_2O (11.0-34.9 nmol vial^{-1}), when O_2 fell below 7.5 µmol vial^{-1}(0.45 µM
373 in the liquid). The two mutants and the wild-type strain showed, however, different denitrification
374 phenotypes regarding their NO_2^- accumulation and the time it took to complete denitrification (seen as an
375 N_2 plateau). The wild-type strain accumulated approximately 50% of the provided 100 µmol NO_3^- vial^{-1} as
376 NO_2^- (62.8 µmol vial^{-1}), supporting its classification as PNA, determined in a separate experiment (Figure
377 S2) where this strain accumulated 44.0 µmol vial^{-1} NO_2^- . In contrast to the wild-type, the Δ*narG* mutant
378 accumulated <1.3 µmol vial^{-1} NO_2^- (Figure 4). It had thus obtained an LNA phenotype similar to the strains
379 *Stutzerimonas frequens* DNSP21 and *S. stutzeri* 28a3 (Figure 1c and Figure S3a), both of which lack *narG*
380 and thus use only Nap for dissimilatory NO_3^- reduction (Table 1). As expected, deleting *narG* slowed

381 denitrification so that the reduction of the provided NO_3^- to N_2 took almost three times longer than for the
382 wild-type (78 h *vs* 28 h). Knocking out the *dnrE* gene had a less severe effect on the time it took to complete
383 denitrification (38 h). However, and contrary to our expectations, the Δ*dnrE* mutant showed increased
384 accumulation of NO_2^- compared to the wild-type, reaching 80.1 ± 4.99 µmol vial^{-1}. The NO_2^- accumulation
385 rates were however almost equal with 5.5 ±0.7 µmol vial^{-1} h^{-1} for the wild-type and 5.5 ± 0.4 µmol vial^{-1} h^{-}
386 ^{1} for the Δ*dnrE* mutant.

387 Competition for electrons between the NO_3^- and NO_2^- reduction pathways

388 To investigate whether competition for electrons between the NO_3^- and NO_2^- reduction pathways influences
389 NO_2^- accumulation, we added NO_3^- to actively NO_2^- reducing cultures. Three strains were studied (ZoBell,
390 FNA; 19SMNA, PNA and JM300, LNA), each representing one of the phenotype groups (Figure 5a-c).
391 The cultures were initially incubated under the denitrifying conditions described above to induce the
392 development of the denitrification proteome, after which the cells were transferred to new anoxic vials
393 (initial OD_{600} 0.3) with medium containing 100 µmol NO_2^- vial^{-1} (corresponding to 2 mM NO_2^- in the
394 medium) (t=0). When approximately one third of the initial NO_2^- had been reduced, 100 µmol vial^{-1} of NO_3^-
395 (corresponding to 2 mM NO_3^- in the medium) was added to the vial. For strain ZoBell (Figure 5a), the
396 addition of NO_3^- to the actively NO_2^- respiring culture led to an immediate shift to NO_3^- respiration and a
397 complete halt of the NO_2^- reduction until all the added NO_3^- had been reduced. This shift is also seen from
398 the plummeting of the NO concentration and the plateauing of N_2. Once all the NO_3^- had been reduced,
399 NO_2^- respiration resumed along with the downstream denitrification steps as seen from the decrease of NO_2^-
400 and the concomitant accumulation of NO (<50 nmol vial^{-1}). N_2 increased until it reached a plateau at
401 approximately 200 µmol N_2-N vial^{-1}, reflecting the complete reduction of the added NO_3^- and NO_2^-.

402 In a similar experiment, strain 19SMN4 (PNA) reduced NO_3^- and NO_2^- simultaneously following
403 supplementation with NO_3^-, and continuously reduced NO_2^- further to N_2, as seen by the constant increase
404 of N_2 and lack of an intermittent N_2 plateau (Figure 5b). NO_3^- was apparently reduced faster than NO_2^-,
405 resulting in a transient accumulation of NO_2^- from 75 to 123 µmol vial^{-1}(thus about half of the added NO_3^-

406) until all the available NO_3^- was depleted. The LNA strain JM300 (Figure 5c) continued to reduce NO_2^-
407 despite the addition of NO_3^-, with no accumulation of NO_2^-. The NO_2^- reduction proceeded without any
408 apparent reduction in rate until all NO_3^- and NO_2^- had been consumed, seen as N_2-N reaching a plateau. As
409 observed with strain ZoBell, the accumulation of NO peaked at ≤ 50 nmol vial^{-1} in experiments with strains
410 19SMN4 or JM300 (Figure 5b-c).

411 Analysis of a possible role of sRNAs in regulating nitrite accumulation

412 We investigated potential regulatory mechanisms underlying the nitrite accumulation phenotype by
413 examining the role of small RNAs (sRNAs). Inclusion of selected sRNAs was based on their previous
414 association to either regulation of the broader nitrogen cycle, to denitrification specifically, to anaerobic
415 regulators, and to regulators located within denitrification gene clusters in *Stutzerimonas* sp. (Lin et al.
416 2015; Zhan et al. 2016; Wang et al. 2022). With these criteria, eight putative sRNAs (crcZ, nfiS, P11, P15,
417 pda200, phrS, prrF1, rsmY) were selected for investigation and overexpression strains constructed.
418 Overexpression has been used to assign function to sRNAs from a wide range of bacterial species and
419 associated processes (Massé and Gottesman 2002; Gaimster et al. 2019). We assessed the NO_2^-
420 accumulation under anaerobic conditions for the sRNA-overexpressing strains (Figure S8). During
421 anaerobic growth, NO_2^- accumulation peaked between 83.2 ± 7.7 and 104.2 ± 0.4 μmol vial^{-1}. However,
422 pairwise Tukey HSD tests revealed no statistically significant differences in NO_2^- accumulation between
423 any of the overexpression strains and the control ($p > 0.05$).

424 Discussion

425 Nitrite accumulation can have significant environmental consequences, as it plays a central role in the
426 emissions of N_2O, NO and HONO from various environments (Bhattarai et al. 2018; Frostegård et al. 2022;
427 Song et al. 2023), and can also hamper N removal efficiency in wastewater plants (Zhou et al. 2011). Despite
428 its importance, variation in patterns of transient NO_2^- accumulation among denitrifying organisms has
429 received relatively little attention, and mechanisms underlying this phenotype remain poorly understood.
430 Our study of eighteen closely related strains revealed a greater diversity in denitrification phenotypes within

431 the genus *Stutzerimonas* than previously recognized, with strains exhibiting full, partial, or low NO_2^--
432 accumulating phenotypes. We identified multiple factors that either individually or in concert contribute to
433 varying levels of transient NO_2^- accumulation in *Stutzerimonas*, including genetic configurations as well as
434 regulatory mechanisms operating at both the transcriptional and post-transcriptional/metabolic levels. The
435 phenotype grouping showed partial congruence with phylogeny (Figure 2): FNA and PNA were
436 phylogenetically intertwined, and in some cases, even strains of the same species belonged to different
437 phenotype groups. The LNA strains were mostly phylogenetically separated from the two other phenotype
438 groups, with one exception (DNSP21). Genome clustering supported these observations, with the exception
439 that strains DNSP21 and 24a75 showed proximity (Figure S4). The limited congruence between phylogeny
440 or genome clustering and NO_2^- accumulation phenotype is consistent with findings from the genus *Thauera*
441 (Liu et al. 2013) and underscores the need for caution against inferring regulatory phenotypes based solely
442 on taxonomic relatedness.

443 The genome survey of denitrification-related genes (Table 1) did not conclusively explain the three
444 phenotype groups, as variations in the gene clusters encoding both dissimilatory NO_3^- and NO_2^- reduction
445 were not consistently associated with specific phenotypes. In contrast, the clusters for NO and N_2O
446 reduction were arranged consistently across all three groups. A previous investigation of bacteria in the
447 genus *Thauera* (Liu et al. 2013) suggested that *nar* plays a key role in NO_2^- accumulation, since strains
448 carrying both the *nar* and *nap* clusters accumulated NO_2^-, while those with only the *nap* cluster did not. In
449 line with this, all *Stutzerimonas* strains classified as FNA and PNA in the present study carried the *nar*
450 genes. However, unlike the *Thauera* strains, the *nar* cluster was also found in all but two of the LNA strains.
451 This suggests that additional mechanisms controlling the expression of denitrification related genes are
452 involved in determining the NO_2^- accumulation levels.

453 To investigate whether transcriptional control mechanisms could explain why the LNA strains
454 possessing both *nar* and *nap* accumulated little or no NO_2^-, we measured transcriptional activity in two such
455 strains. Strain JM300 showed significantly delayed *narG* transcription by approximately 4-6 h compared

456 to other denitrification related genes (Figure 3d), implying that it relied only on Nap for NO_3^- reduction
457 during this period. This slower NO_3^- reduction allowed Nir to maintain pace, preventing NO_2^- accumulation.
458 Interestingly, strain JM300 carries the NO_2^- reductase gene *nirK* in addition to *nirS*, and it cannot be
459 excluded that this contributed to the lack of NO_2^- accumulation. To explore this further, we performed a
460 transcription analysis of the LNA strain DSM 50238, which carries both *napA* and *narG* but only *nirS* for
461 dissimilatory NO_2^- reduction (thus lacking *nirK*). These strains showed the same temporal pattern of
462 transcription as JM300, with a significant delay in *narG* transcription (Figure S5), although copy numbers
463 were lower for DSM 50238, for which real-time PCR was used, compared to the ddPCR analysis used for
464 JM300. Collectively, these results reinforce the role of NarG as a primary factor in determining whether a
465 denitrifier accumulates NO_2^-. This is further supported by the results from the *narG* knock-out mutant,
466 which shifts PNA strain 19SMN4 to a LNA phenotype (Figure 4).

467 While the presence and activity of Nar appear to be significant factors in determining whether a
468 strain accumulates NO_2^-, they do not conclusively explain the difference between the phenotype groups. A
469 primary distinction between the FNA group and the PNA/LNA groups appears to lie in their transcriptional
470 control of *nirS* (Figure 3). The FNA phenotype was characterized by a progressive onset of denitrification,
471 whereas the LNA phenotype showed a rapid and complete onset, similar to reports on *Thauera* strains (Liu
472 et al. 2013). In that study, the FNA strain *Thauera terpenica* showed a low transcription peak of *nirS* shortly
473 before O_2 depletion, but the main transcription was delayed and coincided with the peak of NO_2^-
474 accumulation and depletion of NO_3^-. This precise timing of *nirS* transcription led to the tentative suggestion
475 that NO_3^- interacted with one of the regulatory proteins involved in *nirS* transcription, possibly a repressor
476 protein, though no evidence was provided to support such a mechanism. The present, more detailed analysis
477 revealed a similar transcription pattern in *S. perfectomarina* strain ZoBell. Taken together, the findings
478 suggest that temporal control of transcription plays a major role in the near complete NO_2^- accumulation in
479 FNA strains, although other control mechanisms are likely at play as well.

480 The FNA strains showed an almost complete inhibition of NO_2^- reduction while NO_3^- was present,
481 whereas the PNA strains reduced NO_2^- in the presence of NO_3^-, albeit not at a rate sufficient to immediately

482 reduce the produced NO_2^- as effectively as the LNA strains (Figure 5a-c). This suggests that, in both PNA
483 and LNA organisms, electron flow can occur simultaneously to Nar/Nap and Nir, enabling some Nir activity
484 even when NO_3^- is available. The observed difference in NO_2^- accumulation between FNA and PNA strains
485 is unlikely to be explained by the electron pathway to NarG, via NarHI, being a stronger competitor for
486 electrons than the bc_1 complex in FNA organisms relative to PNA organisms. One notable difference
487 between these two groups is the clade of NirS, with FNA strains possessing clade 1b while PNA strains
488 have clade a. This distinction is accompanied by the presence of the genes *nirT* and *nirB* in the clade 1b
489 cluster, but not in the clade 1a cluster (Table 1). These genes encode tetraheme and diheme *c*-type
490 cytochromes, respectively. NirT is a member of the NapC/NirT family of cytochromes, which are
491 characterized by their electron transfer capacity. In addition, NirT may catalytically activate cytochrome
492 cd_1, potentially serving as an essential activating partner for NirS (Zajicek et al. 2004). Notably, NirT is
493 needed for functional NO_2^- reduction in *S. perfectomarina* strain ZoBell (Jüngst et al. 1991; Härtig and
494 Zumft 1999). The NirT and NirB proteins can apparently form a functional heterodimer, as fused NirTB
495 has been found in other NO_2^- accumulating bacteria, such as *Halomonas* sp. 2A, which was detected in a
496 denitritation bioreactor where denitrifying bacteria supplied NO_2^- for anaerobic ammonium oxidation (Li
497 et al. 2018). The involvement of NirTB in NO_2^- reduction is supported by the location of their genes
498 immediately downstream of *nirS*. However, despite these indications of function, the extent to which NirT
499 and NirB contribute to the near-complete inhibition of NirS activity by NO_3^- in FNA strains remains
500 unresolved.

501 Another difference between the phenotype groups was that the *dnrE* gene was present in all FNA
502 and PNA strains but absent in all LNA strains (Table 1), making it a candidate gene for involvement in NO_2^-
503 accumulation. DnrE belongs to the FNR/CRP family of transcriptional regulators, which sense
504 environmental signals such as O_2 and NO. We hypothesized that knocking out *dnrE* in an FNA or PNA
505 strain would decrease or delay the transcription of *narG*, thereby slowing NO_3^- reduction and reducing NO_2^-
506 accumulation. Contrary to our expectations, the NO_2^- accumulation rate of the PNA strain 19SMN4 deletion
507 mutant remained equal to the wild-type (Figure 4), excluding DnrE from playing a direct regulatory role in

508 NO_2^- accumulation. The *dnrE* gene is located within the *nar* gene cluster, alongside *narXL*. NarXL is a two-
509 component sensor–regulator system that senses NO_3^- and NO_2^- with a higher affinity for NO_3^-, which
510 directly controls the expression of *narG* and *dnrE* (Härtig et al. 1999). Consequently, in the *dnrE* knockout
511 mutant, *narG* expression was maintained, possibly through NarXL, despite the absence of *dnrE*, which
512 makes it challenging to elucidate the specific role of *dnrE* in regulating NO_2^- accumulation. Despite high
513 homology among the Dnr regulatory proteins DnrE, DnrS and DnrD (>40% identity and >90% coverage),
514 their functions are distinct: DnrS senses O_2, DnrD senses NO, while the role of DnrE remains unknown.
515 The regulation of *dnrE* appears to be conserved in all FNA and PNA strains, as indicated by a highly
516 conserved upstream intergenic region containing two putative NarL binding sites, a ribosome binding site
517 (RBS), and two promoters (Figure S9). This conservation suggests a similar regulatory mechanism
518 controlling *dnrE* expression. Consistent with Vollack et al. (1999), no FNR-box was detected upstream of
519 *dnrE*, suggesting that the main anaerobic regulator, Anr, which senses O_2, may not directly regulate *dnrE*.
520 Nevertheless, *dnrE* transcription increases in the presence of both NO_3^- and O_2, indicating that another
521 oxygen-sensitive factor may trigger its expression. This suggests that DnrE is involved in a complex,
522 multilayered regulatory network (Spiro 2012).

523 In our search for additional regulatory mechanisms influencing denitrification, we examined the
524 potential role of small RNAs (sRNAs) in modulating NO_2^- accumulation in the FNA strain *S.*
525 *perfectomarina* ZoBell. Candidate sRNAs were selected based on their conservation across *Pseudomonas*
526 species, their genomic proximity to denitrification gene clusters, and previous associations with nitrogen
527 metabolism. Although several candidates were successfully overexpressed under anaerobic conditions, no
528 significant changes in NO_2^- accumulation were observed, suggesting that none of the selected sRNAs
529 directly regulates denitrification under the tested conditions although mutational analyses would be needed
530 to fully rule them out. These findings highlight the limitations of a candidate-based approach and emphasize
531 the need for broader transcriptomic analyses. In particular, *de novo* RNA-seq analyses, comparing closely

532 related *Stutzerimona*s strains exhibiting different NO_2^- accumulation phenotypes, could provide valuable
533 insight into the denitrification specific transcriptional landscape.

534 Taken together, the results enhance the understanding of how variations in regulatory phenotypes
535 may influence NO_2^- accumulation across various environments and highlight how organisms optimize
536 energy savings by temporarily blocking steps in the denitrification pathway, albeit at the cost of providing
537 substrates to competing populations. Importantly, these findings have significant implications for various
538 biotechnological approaches. FNA strains can supply NO_2^- for denitratation in anammox wastewater
539 treatment (Zhuang et al. 2022). NNA strains, on the other hand, may be candidates for engineering soil
540 microbiomes for N_2O mitigation (Hiis et al. 2024), since they maintain low levels of all denitrification
541 intermediates.

542

543 Conclusions

544 Our study demonstrates substantial variation in denitrification phenotypes among closely
545 related *Stutzerimonas* strains, driven by a complex interplay of genetic, transcriptional, and post-
546 transcriptional mechanisms that influence NO_2^- accumulation. We found that even organisms with a
547 complete set of denitrification genes can act as partial denitrifiers by temporarily constraining specific steps,
548 as seen in the FNA strains. This likely conserves energy, providing an advantage in environments with
549 fluctuating O_2 levels where full denitrification is only occasionally required. Similar to classical "partial
550 denitrifiers", which lack certain genes and therefore share metabolic tasks (Roothans et al. 2025), FNA-like
551 organisms rely on community members capable of consuming NO_2^-, including other denitrifiers, DNRA
552 organisms (performing dissimilatory NO_3^-/NO_2^- reduction to ammonia), or NO_2^- oxidizers if O_2 is available,
553 to keep NO_2^- concentrations non-toxic. This collaboration helps prevent the buildup of NO_2^- and the
554 formation of environmentally harmful byproducts such as NO and N_2O, including those from abiotic NO_2^-
555 reactions (Lim et al. 2018). While the presence and timing of *narG* transcription were identified as key

556 determinants of transient NO_2^- accumulation, other factors—including the type of *nirS* and
557 associated *nirT/nirB* genes, as well as competition for electrons between Nar and Nir pathways—also play
558 important roles. Our results highlight the limitations of predicting NO_2^- accumulation potential based solely
559 on taxonomy or gene presence. Overall, these findings underscore the complexity of denitrification
560 regulation and emphasize the need for integrative approaches combining microbial physiology,
561 biochemistry, and transcriptomics to link genotype to denitrification phenotypes. A deeper understanding
562 of these mechanisms is essential for managing NO_2^- and related intermediates in both environmental and
563 engineered systems, such as wastewater treatment, and for supporting efforts to mitigate greenhouse gas
564 emissions.
565

566 **Author contributions**

567 **Martin Menestreau:** investigations, formal analysis, visualization, data interpretation, writing – original
568 draft, writing – review and editing. **Daniel A. Milligan:** preliminary investigations (gas kinetics,
569 transcription, genome analyses), writing – early draft. **Louise B. Sennett:** data analysis (statistics), writing-
570 - editing. **Linda Bergaust:** data interpretation, writing – review and editing. **Lars R. Bakken** data
571 interpretation, writing – review and editing. **Gary Rowley:** supervision of sRNA work, writing – review
572 and editing. **Morten Kjos:** supervision of CRISPR analyses, writing – review and editing. **James P.**
573 **Shapleigh:** data analysis (phylogeny), data interpretation, validation, writing – review and editing. **Åsa**
574 **Frostegård:** conceptualization, funding acquisition, supervision, project administration, data
575 interpretation, validation, writing – original draft, writing – review and editing. All authors contributed to
576 the article and approved the submitted version.
577

578 **Acknowledgements**

579 This work was supported by the Research Council of Norway, project no. 325770 (awarded to Å.F.).

580 **Conflicts of interest**

581 The authors declare no conflicts of interest

Data availability statement

The gas kinetics and transcription data that support the findings of this study are available on request from the corresponding author.

References

Aziz, R. K., Bartels, D., Best, A. A., DeJongh, M., Disz, T., Edwards, R. A., … Zagnitko, O. (2008). The RAST server: Rapid annotations using subsystems technology. *BMC Genomics, 9*(1), 75. https://doi.org/10.1186/1471-2164-9-75

Bakken, L. R., Bergaust, L., Liu, B., & Frostegård, Å. (2012). Regulation of denitrification at the cellular level: A clue to the understanding of N_2O emissions from soils. *Philosophical Transactions of the Royal Society B: Biological Sciences, 367*(1593), 1226–1234. https://doi.org/10.1098/rstb.2011.0321

Bergaust, L., Mao, Y., Bakken, L. R., & Frostegård, Å. (2010). Denitrification response patterns during the transition to anoxic respiration and posttranscriptional effects of suboptimal pH on nitrogen oxide reductase in *Paracoccus denitrificans*. *Applied and Environmental Microbiology, 76*(19), 6387–6396. https://doi.org/10.1128/AEM.00608-10

Berks, B. C., Ferguson, S. J., Moir, J. W., & Richardson, D. J. (1995). Enzymes and associated electron transport systems that catalyze the respiratory reduction of nitrogen oxides and oxyanions. *Biochimica et Biophysica Acta (BBA) - Bioenergetics, 1232*, 97–173. https://doi.org/10.1016/0005-2728(95)00092-5

Bhattarai, H. R., Virkajärvi, P., Yli-Pirilä, P., & Maljanen, M. (2018). Emissions of atmospherically important nitrous acid (HONO) gas from northern grassland soil increases in the presence of nitrite (NO_2^-). *Agriculture, Ecosystems & Environment, 256*, 194–199. https://doi.org/10.1016/j.agee.2018.01.017

Braman, R. S., & Hendrix, S. A. (1989). Nanogram nitrite and nitrate determination in environmental and biological materials by vanadium(III) reduction with chemiluminescence detection. *Analytical Chemistry, 61*(24), 2715–2718. https://doi.org/10.1021/ac00199a007

Carlson, C. A., & Ingraham, J. L. (1983). Comparison of denitrification by *Pseudomonas stutzeri, Pseudomonas aeruginosa*, and *Paracoccus denitrificans*. *Applied and Environmental Microbiology, 45*(4), 1247–1253. https://doi.org/10.1128/aem.45.4.1247-1253.1983

Chen, J., & Strous, M. (2013). Denitrification and aerobic respiration, hybrid electron transport chains and co-evolution. *Biochimica et Biophysica Acta (BBA) - Bioenergetics, 1827*(2), 136–144. https://doi.org/10.1016/j.bbabio.2012.10.002

Chen, W., Zhang, Y., Zhang, Y., Pi, Y., Gu, T., Song, L., Wang, Y., & Ji, Q. (2018). CRISPR/Cas9-based genome editing in *Pseudomonas aeruginosa* and cytidine deaminase-mediated base editing in Pseudomonas species. *iScience, 6*, 222–231. https://doi.org/10.1016/j.isci.2018.07.024

Chislett, M., Guo, J., Bond, P. L., Wang, Y., Donose, B. C., & Yuan, Z. (2022). Reactive nitrogen species from free nitrous acid (FNA) cause cell lysis. *Water Research*, *217*, 118401. https://doi.org/10.1016/j.watres.2022.118401

Choi, K.-H., Kumar, A., & Schweizer, H. P. (2006). A 10-min method for preparation of highly electrocompetent *Pseudomonas aeruginosa* cells: Application for DNA fragment transfer between

chromosomes and plasmid transformation. *Journal of Microbiological Methods, 64*(3), 391–397. https://doi.org/10.1016/j.mimet.2005.06.001

Cole, J. A. (2025). Nitrate reduction for survival in a nanomolar world, not the millimolar world of a laboratory. In *Advances in Microbial Physiology* (Vol. 87, pp. 79–117). Elsevier. https://doi.org/10.1016/bs.ampbs.2025.07.005

Concordet, J.-P., & Haeussler, M. (2018). CRISPOR: Intuitive guide selection for CRISPR/Cas9 genome editing experiments and screens. *Nucleic Acids Research, 46*(W1), W242–W245. https://doi.org/10.1093/nar/gky354

Cox, R. D. (1980). Determination of nitrate and nitrite at the parts per billion level by chemiluminescence. *Analytical Chemistry, 52*(2), 332–335. https://doi.org/10.1021/ac50052a028

Decleyre, H., Tytgat, B., & Anne, W. (2016). Highly diverse *nirK* genes comprise two major clades that harbour ammonium-producing denitrifiers. *BMC Genomics, 17*(1), 155. https://doi.org/10.1186/s12864-016-2465-0

Ebert, M., Laaß, S., Thürmer, A., Roselius, L., Eckweiler, D., Daniel, R., Härtig, E., & Jahn, D. (2017). FnrL and three Dnr regulators are used for the metabolic adaptation to low oxygen tension in *Dinoroseobacter shibae*. *Frontiers in Microbiology, 8*, 642. https://doi.org/10.3389/fmicb.2017.00642

Edgar, R. C. (2004). MUSCLE: Multiple sequence alignment with high accuracy and high throughput. *Nucleic Acids Research, 32*(5), 1792–1797. https://doi.org/10.1093/nar/gkh340

Frostegård, Å., Vick, S. H. W., Lim, N. Y. N., Bakken, L. R., & Shapleigh, J. P. (2022). Linking meta-omics to the kinetics of denitrification intermediates reveals pH-dependent causes of N_2O emissions and nitrite accumulation in soil. *The ISME Journal, 16*(1), 26–37. https://doi.org/10.1038/s41396-021-01045-2

Gaimster, H., Alston, M., Richardson, D. J., Gates, A. J., & Rowley, G. (2018). Transcriptional and environmental control of bacterial denitrification and N_2O emissions. *FEMS Microbiology Letters, 365*(5). https://doi.org/10.1093/femsle/fnx277

Gaimster, H., Hews, C. L., Griffiths, R., Soriano-Laguna, M. J., Alston, M., Richardson, D. J., Gates, A. J., & Rowley, G. (2019). A central small RNA regulatory circuit controlling bacterial denitrification and N_2O emissions. *mBio, 10*(4), e01165-19. https://doi.org/10.1128/mBio.01165-19

Gao, Y., Mania, D., Mousavi, S. A., Lycus, P., Arntzen, M. Ø., Woliy, K., Lindström, K., Shapleigh, J. P., Bakken, L. R., & Frostegård, Å. (2021). Competition for electrons favors N_2O reduction in denitrifying *Bradyrhizobium* isolates. *Environmental Microbiology, 23*(4), 2244–2259. https://doi.org/10.1111/1462-2920.15404

Gomila, M., Mulet, M., García-Valdés, E., & Lalucat, J. (2022). Genome-based taxonomy of the genus *Stutzerimonas* and proposal of *S. frequens* sp. nov. and *S. degradans* sp. nov. and emended descriptions of *S. perfectomarina* and *S. chloritidismutans*. *Microorganisms, 10*(7), 1363. https://doi.org/10.3390/microorganisms10071363

Guindon, S., Dufayard, J.-F., Lefort, V., Anisimova, M., Hordijk, W., & Gascuel, O. (2010). New algorithms and methods to estimate maximum-likelihood phylogenies: Assessing the performance of PhyML 3.0. *Systematic Biology, 59*(3), 307–321. https://doi.org/10.1093/sysbio/syq010

Härtig, E., Schiek, U., Vollack, K.-U., & Zumft, W. G. (1999). Nitrate and nitrite control of respiratory nitrate reduction in denitrifying *Pseudomonas stutzeri* by a two-component regulatory system homologous to NarXL of *Escherichia coli*. *Journal of Bacteriology, 181*(12), 3658–3665. https://doi.org/10.1128/JB.181.12.3658-3665.1999

Härtig, E., & Zumft, W. G. (1999). Kinetics of *nirS* expression (cytochrome cd1 nitrite reductase) in *Pseudomonas stutzeri* during the transition from aerobic respiration to denitrification: Evidence for a denitrification-specific nitrate- and nitrite-responsive regulatory system. *Journal of Bacteriology, 181*(1), 161–166. https://doi.org/10.1128/JB.181.1.161-166.1999

Highton, M. P., Bakken, L. R., Dörsch, P., Molstad, L., & Morales, S. E. (2022). Nitrite accumulation and impairment of N_2O reduction explains contrasting soil denitrification phenotypes. *Soil Biology and Biochemistry, 166*, 108529. https://doi.org/10.1016/j.soilbio.2021.108529

Hiis, E. G., Vick, S. H. W., Molstad, L., Røsdal, K., Jonassen, K. R., Winiwarter, W., & Bakken, L. R. (2024). Unlocking bacterial potential to reduce farmland N_2O emissions. *Nature*, *630*(8016), 421–428. https://doi.org/10.1038/s41586-024-07464-3

Jones, C. M., Stres, B., Rosenquist, M., & Hallin, S. (2008). Phylogenetic analysis of nitrite, nitric oxide, and nitrous oxide respiratory enzymes reveal a complex evolutionary history for denitrification. *Molecular Biology and Evolution, 25*(9), 1955–1966. https://doi.org/10.1093/molbev/msn146

Jüngst, A., Wakabayashi, S., Matsubara, H., & Zumft, W. G. (1991). The *nirSTBM* region coding for cytochrome cd1-dependent nitrite respiration of *Pseudomonas stutzeri* consists of a cluster of mono-, di-, and tetraheme proteins. *FEBS Letters, 279*(2), 205–209. https://doi.org/10.1016/0014-5793(91)80150-2

Kuypers, M. M. M., Marchant, H. K., & Kartal, B. (2018). The microbial nitrogen-cycling network. *Nature Reviews Microbiology, 16*(5), 263–276. https://doi.org/10.1038/nrmicro.2018.9

Lalucat, J., Bennasar, A., Bosch, R., García-Valdés, E., & Palleroni, N. J. (2006). Biology of *Pseudomonas stutzeri*. *Microbiology and Molecular Biology Reviews, 70*(2), 510–547. https://doi.org/10.1128/MMBR.00047-05

Lalucat, J., Gomila, M., Mulet, M., Zaruma, A., & García-Valdés, E. (2022). Past, present and future of the boundaries of the *Pseudomonas* genus: Proposal of *Stutzerimonas* gen. nov. *Systematic and Applied Microbiology, 45*(1), 126289. https://doi.org/10.1016/j.syapm.2021.126289

Li, W., Li, H., Liu, Y., Zheng, P., & Shapleigh, J. P. (2018). Salinity-aided selection of progressive onset denitrifiers as a means of providing nitrite for anammox. *Environmental Science & Technology, 52*(18), 10665–10672. https://doi.org/10.1021/acs.est.8b02314

Li, X., Yang, Z., Wang, Z., Li, W., Zhang, G., & Yan, H. (2022). Comparative genomics of *Pseudomonas stutzeri* complex: Taxonomic assignments and genetic diversity. *Frontiers in Microbiology, 12*, 755874. https://doi.org/10.3389/fmicb.2021.755874

Lim, N. Y. N., Frostegård, Å., & Bakken, L. R. (2018). Nitrite kinetics during anoxia: The role of abiotic reactions versus microbial reduction. *Soil Biology and Biochemistry, 119*, 203–209. https://doi.org/10.1016/j.soilbio.2018.01.006

Lim, N. Y. N., Roco, C. A., & Frostegård, Å. (2016). Transparent DNA/RNA co-extraction workflow protocol suitable for inhibitor-rich environmental samples that focuses on complete DNA removal for transcriptomic analyses. *Frontiers in Microbiology, 7*, 1588. https://doi.org/10.3389/fmicb.2016.01588

Lin, M., Yan, Y., Lu, W., Zhan, Y., Zhang, Y., & Elmerich, C. (2015). Regulatory coupling of nitrogen and carbon metabolism in nitrogen-fixing *Pseudomonas stutzeri* A1501. In F. J. De Bruijn (Ed.), *Biological nitrogen fixation* (1st ed., pp. 109–120). Wiley. https://doi.org/10.1002/9781119053095.ch10

Liu, B., Mao, Y., Bergaust, L., Bakken, L. R., & Frostegård, Å. (2013). Strains in the genus *Thauera* exhibit remarkably different denitrification regulatory phenotypes. *Environmental Microbiology, 15*(10), 2816–2828. https://doi.org/10.1111/1462-2920.12142

Lycus, P., Lovise Bøthun, K., Bergaust, L., Peele Shapleigh, J., Reier Bakken, L., & Frostegård, Å. (2017). Phenotypic and genotypic richness of denitrifiers revealed by a novel isolation strategy. *The ISME Journal, 11*(10), 2219–2232. https://doi.org/10.1038/ismej.2017.82

Lycus, P., Soriano-Laguna, M. J., Kjos, M., Richardson, D. J., Gates, A. J., Milligan, D. A., Frostegård, Å., Bergaust, L., & Bakken, L. R. (2018). A bet-hedging strategy for denitrifying bacteria curtails their release of N_2O. *Proceedings of the National Academy of Sciences, 115*(46), 11820–11825. https://doi.org/10.1073/pnas.1805000115

Mania, D., Woliy, K., Degefu, T., & Frostegård, Å. (2020). A common mechanism for efficient N_2O reduction in diverse isolates of nodule-forming bradyrhizobia. *Environmental Microbiology, 22*(1), 17–31. https://doi.org/10.1111/1462-2920.14731

Massé, E., & Gottesman, S. (2002). A small RNA regulates the expression of genes involved in iron metabolism in *Escherichia coli*. *Proceedings of the National Academy of Sciences, 99*(7), 4620–4625. https://doi.org/10.1073/pnas.032066599

Moeller, S., Payá, G., Bonete, M.-J., Gates, A. J., Richardson, D. J., Esclapez, J., & Rowley, G. (2021). Microbial small RNAs – The missing link in the nitrogen cycle? *Frontiers in Environmental Science, 9*, 660055. https://doi.org/10.3389/fenvs.2021.660055

Molstad, L., Dörsch, P., & Bakken, L. R. (2007). Robotized incubation system for monitoring gases (O_2, NO, N_2O, N_2) in denitrifying cultures. *Journal of Microbiological Methods, 71*(3), 202–211. https://doi.org/10.1016/j.mimet.2007.08.011

Molstad, L., Dörsch, P., & Bakken, L. R. (2016). Improved robotized incubation system for gas kinetics in batch cultures. Unpublished. https://doi.org/10.13140/RG.2.2.30688.07680

Philippot, L. (2002). Denitrifying genes in bacterial and archaeal genomes. *Biochimica et Biophysica Acta (BBA) - Gene Structure and Expression, 1577*(3), 355–376. https://doi.org/10.1016/S0167-4781(02)00420-7

Pold, G., Bonilla-Rosso, G., Saghaï, A., Strous, M., Jones, C. M., & Hallin, S. (2024). Phylogenetics and environmental distribution of nitric oxide-forming nitrite reductases reveal their distinct functional and ecological roles. *ISME Communications, 4*(1), ycae020. https://doi.org/10.1093/ismeco/ycae020

Richardson, D. (2025). Life on oxidized nitrogen: The biochemistry and physiology of prokaryotic life supported by the nitrate-nitrite redox couple. In *Advances in Microbial Physiology* (Vol. 87, pp. 11–77). Elsevier. https://doi.org/10.1016/bs.ampbs.2025.07.004

Roothans, N., Van Loosdrecht, M. C. M., & Laureni, M. (2025). Metabolic labour division trade-offs in denitrifying microbiomes. *The ISME Journal, 19*(1), wraf020. https://doi.org/10.1093/ismejo/wraf020

Shapleigh, J. P. (2013). Denitrifying prokaryotes. In E. Rosenberg, E. F. DeLong, S. Lory, E. Stackebrandt, & F. Thompson (Eds.), *The Prokaryotes* (pp. 405–425). Springer Berlin Heidelberg. https://doi.org/10.1007/978-3-642-30141-4_71

Sievers, F., Wilm, A., Dineen, D., Gibson, T. J., Karplus, K., Li, W., Lopez, R., McWilliam, H., Remmert, M., Söding, J., Thompson, J. D., & Higgins, D. G. (2011). Fast, scalable generation of high-quality protein multiple sequence alignments using Clustal Omega. *Molecular Systems Biology, 7*(1), 539. https://doi.org/10.1038/msb.2011.75

Sistrom, W. R. (1960). A requirement for sodium in the growth of *Rhodopseudomonas spheroides*. *Journal of General Microbiology, 22*(3), 778–785. https://doi.org/10.1099/00221287-22-3-778

Sommer, M., Xie, H., & Michel, H. (2017). *Pseudomonas stutzeri* as an alternative host for membrane proteins. *Microbial Cell Factories, 16*(1), 157. https://doi.org/10.1186/s12934-017-0771-0

Song, M., Zhao, X., Liu, P., Mu, J., He, G., Zhang, C., Tong, S., Xue, C., Zhao, X., Ge, M., & Mu, Y. (2023). Atmospheric NOx oxidation as major sources for nitrous acid (HONO). *NPJ Climate and Atmospheric Science, 6*(1), 30. https://doi.org/10.1038/s41612-023-00357-8

Spiro, S. (2007). Regulators of bacterial responses to nitric oxide. *FEMS Microbiology Reviews, 31*(2), 193–211. https://doi.org/10.1111/j.1574-6976.2006.00061.x

Spiro, S. (2012). Nitrous oxide production and consumption: Regulation of gene expression by gas-sensitive transcription factors. *Philosophical Transactions of the Royal Society B: Biological Sciences, 367*(1593), 1213–1225. https://doi.org/10.1098/rstb.2011.0309

Trunk, K., Benkert, B., Quäck, N., Münch, R., Scheer, M., Garbe, J., Jänsch, L., Trost, M., Wehland, J., Buer, J., Jahn, M., Schobert, M., & Jahn, D. (2010). Anaerobic adaptation in *Pseudomonas aeruginosa*: Definition of the Anr and Dnr regulons. *Environmental Microbiology, 12*(6), 1719–1733. https://doi.org/10.1111/j.1462-2920.2010.02252.x

Vaccaro, B. J., Thorgersen, M. P., Lancaster, W. A., Price, M. N., Wetmore, K. M., Poole, F. L., Deutschbauer, A., Arkin, A. P., & Adams, M. W. W. (2016). Determining roles of accessory genes in denitrification by mutant fitness analyses. *Applied and Environmental Microbiology, 82*(1), 51–61. https://doi.org/10.1128/AEM.02602-15

Van Cleemput, O., & Samater, A. H. (1995). Nitrite in soils: Accumulation and role in the formation of gaseous N compounds. *Fertilizer Research, 45*(1), 81–89. https://doi.org/10.1007/BF00749884

Vollack, K., Härtig, E., Körner, H., & Zumft, W. G. (1999). Multiple transcription factors of the FNR family in denitrifying Pseudomonas stutzeri: Characterization of four fnr-like genes, regulatory responses and cognate metabolic processes. Molecular Microbiology, 31(6), 1681–1694. https://doi.org/10.1046/j.1365-2958.1999.01302.x

Vollack, K.-U., Xie, J., Härtig, E., Römling, U., & Zumft, W. G. (1998). Localization of denitrification genes on the chromosomal map of Pseudomonas aeruginosa. Microbiology, 144(2), 441–448. https://doi.org/10.1099/00221287-144-2-441

Wang, M., Liang, Y., Li, F., Shen, S., Huang, X., & Sun, Y. (2022). Enhancement of biological denitrification by the addition of novel sRNA Pda200 under antibiotic pressure. Bioresource Technology, 365, 128113. https://doi.org/10.1016/j.biortech.2022.128113

Wittorf, L., Jones, C. M., Bonilla-Rosso, G., & Hallin, S. (2018). Expression of nirK and nirS genes in two strains of Pseudomonas stutzeri harboring both types of NO-forming nitrite reductases. Research in Microbiology, 169(6), 343–347. https://doi.org/10.1016/j.resmic.2018.04.010

Zajicek, R. S., Allen, J. W. A., Cartron, M. L., Richardson, D. J., & Ferguson, S. J. (2004). Paracoccus pantotrophus NapC can reductively activate cytochrome cd1 nitrite reductase. FEBS Letters, 565(1–3), 48–52. https://doi.org/10.1016/j.febslet.2004.03.072

Zerbino, D. R., & Birney, E. (2008). Velvet: Algorithms for de novo short read assembly using de Bruijn graphs. Genome Research, 18(5), 821–829. https://doi.org/10.1101/gr.074492.107

Zhan, Y., Yan, Y., Deng, Z., Chen, M., Lu, W., Lu, C., Shang, L., Yang, Z., Zhang, W., Wang, W., Li, Y., Ke, Q., Lu, J., Xu, Y., Zhang, L., Xie, Z., Cheng, Q., Elmerich, C., & Lin, M. (2016). The novel regulatory ncRNA, NfiS, optimizes nitrogen fixation via base pairing with the nitrogenase gene nifK mRNA in Pseudomonas stutzeri A1501. Proceedings of the National Academy of Sciences, 113(30). https://doi.org/10.1073/pnas.1604514113

Zhou, Y., Oehmen, A., Lim, M., Vadivelu, V., & Ng, W. J. (2011). The role of nitrite and free nitrous acid (FNA) in wastewater treatment plants. Water Research, 45(15), 4672–4682. https://doi.org/10.1016/j.watres.2011.06.025

Zhuang, J.-L., Sun, X., Zhao, W.-Q., Zhang, X., Zhou, J.-J., Ni, B.-J., Liu, Y.-D., Shapleigh, J. P., & Li, W. (2022). The anammox-coupled partial-denitrification process in an integrated granular sludge and fixed-biofilm reactor developed for mainstream wastewater treatment: Performance and community structure. Water Research, 210, 117964. https://doi.org/10.1016/j.watres.2021.117964

Zumft, W. G. (1997). Cell biology and molecular basis of denitrification. Microbiology and Molecular Biology Reviews, 61(4), 533–616. https://doi.org/10.1128/mmbr.61.4.533-616.1997

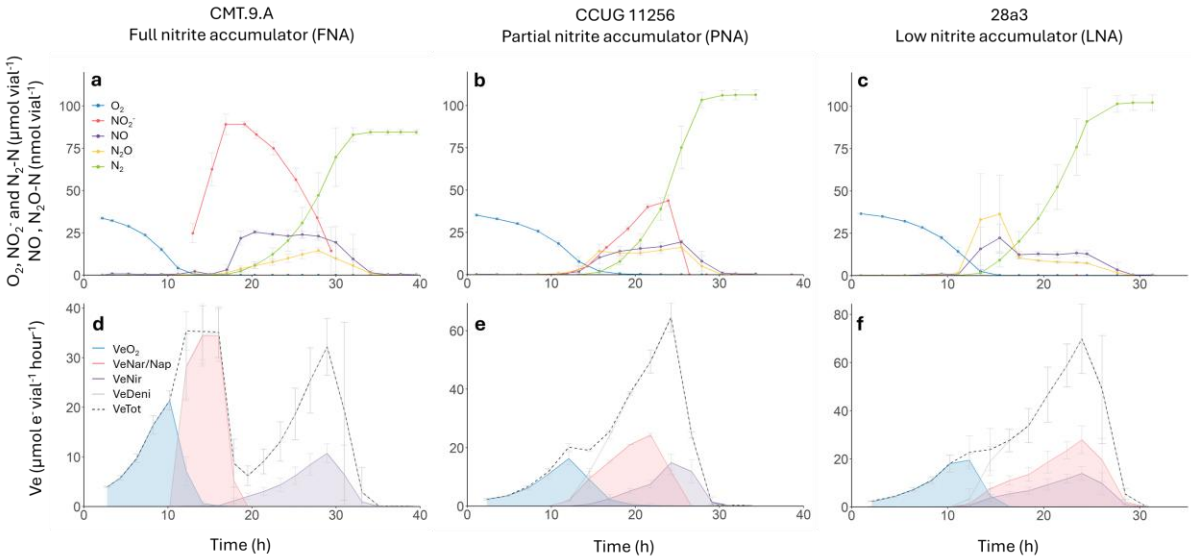

Figure 1. Denitrification kinetics (a–c) and electron flow rates to reductases (d–f) during and after the transition from aerobic respiration to denitrification. Strains were incubated at 20 °C in 120 mL medical vials containing 50 mL Sistrom's mineral medium, supplemented with KNO_3 to an initial concentration of 2 mM (100 µmol vial^{-1}), with He and 1% O_2 in the headspace. The panels show the results for three strains representing the FNA, PNA, and LNA groups. The upper panels show the measured NO_2^- and gases and the lower panels show the calculated rate of electron flow to O_2 (blue), NO_3^- (red), and NO_2^- (purple), with the total electron flow shown as a dashed line. All graphs show mean values from three independent replicates (n = 3); error bars represent standard deviation.

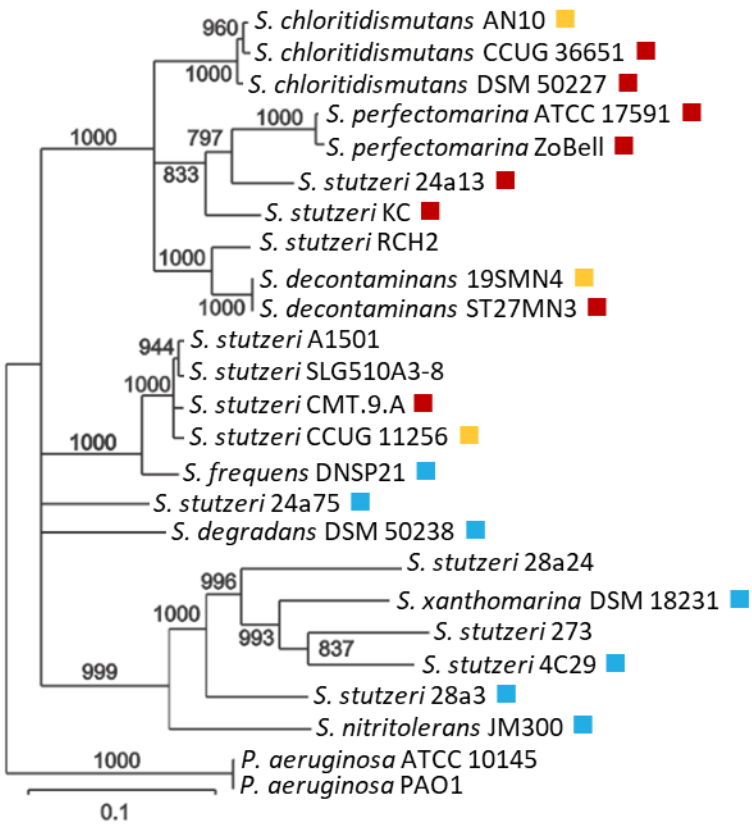

Figure 2. Maximum likelihood phylogenetic tree of selected *Stutzerimonas* strains and their NO_2^- accumulation phenotype. The three NO_2^- accumulation groups are indicated by different colors in the phylogenetic tree. Red: Full NO_2^- accumulators (FNA); reduced almost all available NO_3^- before reducing any NO_2^-. Yellow: Partial NO_2^- accumulators (PNA); transient accumulation of NO_2^- reaching approximately 40-60% of the amount of added NO_3^- Blue: Low NO_2^- accumulators (LNA); 0-20% of the reduced NO_3^- was transiently accumulated as NO_2^-. The phylogenetic analysis was a multilocus sequence analysis (MLSA) based on concatenated sequences of partial 16S rRNA and full *gyrB* and *rpoD* gene sequences. In addition to the strains analyzed for denitrification phenotypes, some other strains were included for which complete genome sequence data were publicly available. Only branches with bootstrap values ≥ 700 (of 1000) are shown. The strains were until recently included in a species complex encompassing the former *Pseudomonas stutzeri* and closely related strains (Li et al. 2022) but were recently circumscribed into several species of the novel genus *Stutzerimonas* (Laculat et al. 2022; Gomila et al. 2022). A list of the strains, including their origin and culture collection numbers, is provided in Table S1. A more detailed tree based on genome clustering, including all presently available *Stutzerimonas* genomes, is found in Figure S4.

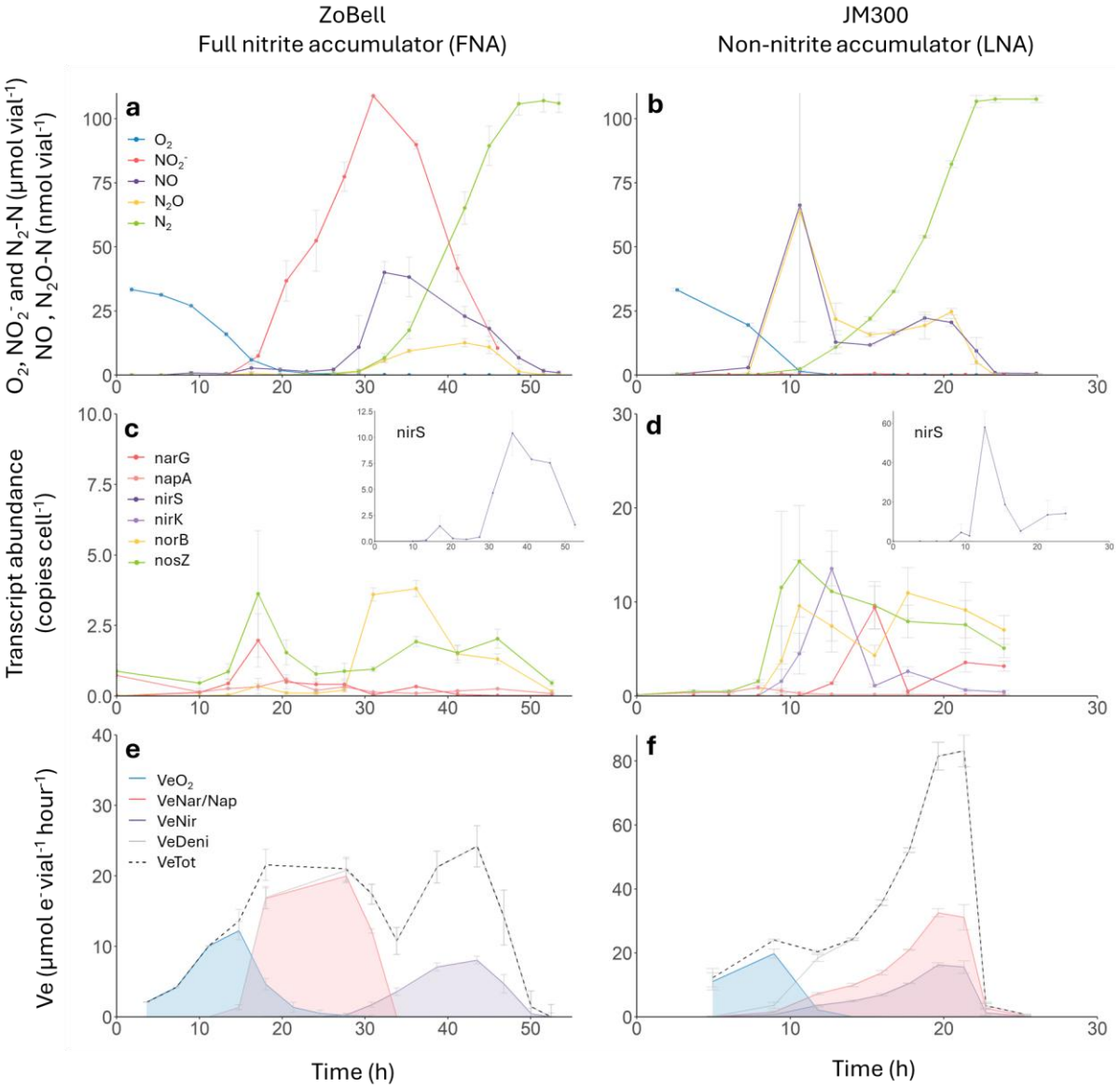

Figure 3. Denitrification kinetics, gene transcription and electron flow in the FNA strain ZoBell and the LNA strain JM300, switching from aerobic to anaerobic respiration. The panels show measured NO_2^- and gases (a, b), the denitrification gene transcription (c, d), and electron flow rates to reductases (e, f) during and after the transition from aerobic respiration to denitrification. Strains were incubated at 20 °C in 120 mL medical vials containing 50 mL Sistrom's mineral medium, supplemented with KNO_3 to an initial concentration of 2 mM (100 µmol vial^{-1}), with He and 1% O_2 in the headspace. Graphs show mean values from six independent replicates (n = 6); error bars represent standard deviation.

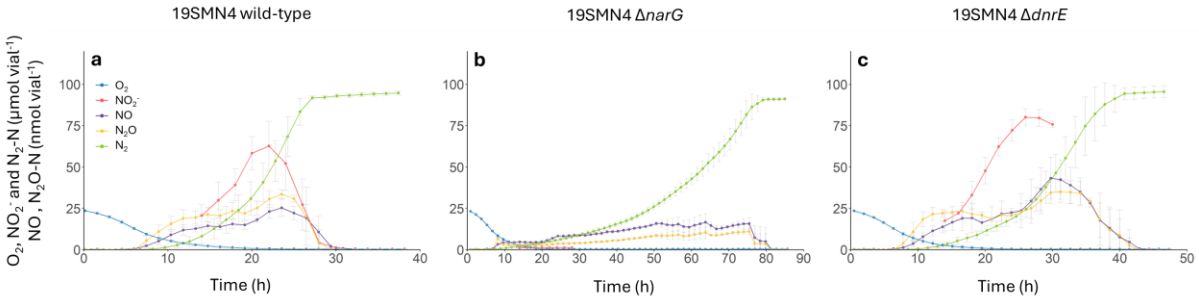

Figure 4. Effect of deleting *narG* and *dnrE* on the phenotype of the PNA strain *Stutzerimonas decontaminans* 19SMN4. The panels show the measured NO_2^- and gases during and after the transition from aerobic respiration to denitrification for the wild type (a), *narG* deletion mutant (b) and *dnrE* deletion mutant (c). Strains were incubated at 20 °C in 120 mL medical vials containing 50 mL Sistrom's mineral medium, supplemented with KNO_3 to an initial concentration of 2 mM (100 µmol vial^{-1}), with He and 1% O_2 in the headspace. Graphs show mean values from three independent replicates (n = 3); error bars represent standard deviation.

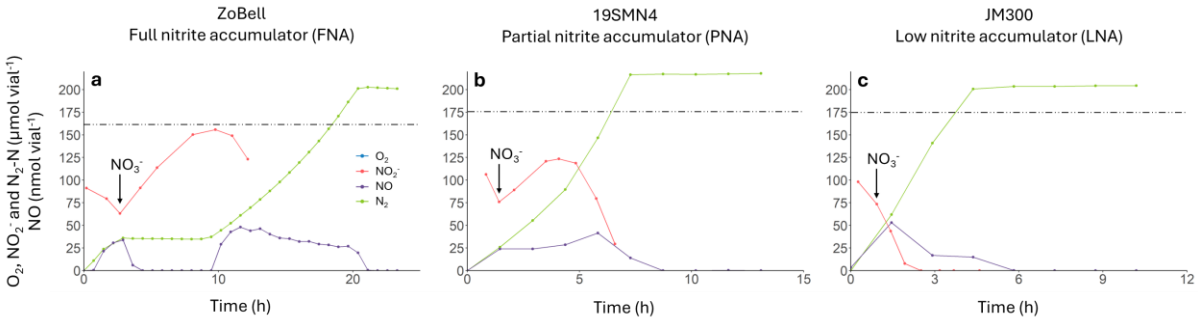

Figure 5. Competition for electrons between NO_3^- and NO_2^- reduction pathways. Results for three *Stutzerimonas* strains, each representing one of the three nitrite accumulation phenotypes (a–c). Experiments were performed in biological triplicates (n = 3). The timing of NO_3^- addition varied between replicate vials; therefore, one representative replicate is shown here, while the other replicates, which displayed very similar patterns, are presented in Fig. S7. Cultures were pre-grown anoxically (100% He headspace) in Sistrom's medium with NO_3^- to induce full denitrification proteomes, then transferred at t = 0 to fresh anoxic vials containing only 2 mM NO_2^- (100 µmol vial^{-1}). When approximately one-third of the NO_2^- was reduced, 100 µmol of NO_3^- (corresponding to 2 mM in the medium) was added (indicated by the arrow).

		NO_3^- to NO_2^-			NO_2^- to NO				NO to N_2O	N_2O to N_2	Maximum Denitrification intermediates accumulation (NO_2^- µmol vial^{-1}, NO and N_2O nmol vial^{-1})						
		Periplasmic nitrate red.	Membrane-bound nitrate red.		Cytochrome cd_1-nitrite red.			Copper nitrite red.	c-Nitric oxide red.	Nitrous oxide red. clade I							
Group	Strain	*napABCDE*	*narGHJIKMXL*	*dnrE*	NirS clade	*nirJENY*	*nirTB*	NirK clade	*norBCD*	*nosRZDFYL*	Max NO_2^-		Max NO		Max N_2O		
FNA	CCUG 36651	+	+	+	Clade 1b	downstream	+	clade II	+	+	96.5 ± 0.6	a	39.3 ± 0.3	abc	22.1 ± 1.0	a	
	DSM 50227	+	+	+	Clade 1b	downstream	+	clade II	+	+	101.4 ± 5.7		62.5 ± 15.5		7.7 ± 1.7		
	ATCC 17591	+	+	+	Clade 1b	downstream	+	clade II	+	+	92.9 ± 0.4		26.5 ± 4.2		15.8 ± 2.2		
	ZoBell	+	+	+	Clade 1b	downstream	+	–	+	+	108.8 ± 0.25		70.5 ± 5.0		11.8 ± 1.2		
	24a13	+	+	+	Clade 1b	downstream	+	clade II	+	+	71.7 ± 5.7		32.1 ± 2.8		19.7 ± 1.3		
	KC	+	+	+	Clade 1b	downstream	+	–	+	+	96.7 ± 0.2		25.0 ± 0.6		13.7 ± 0.2		
	ST27MN3	+	+	+	Clade 1b	downstream	+	–	+	+	101.5 ± 6.0		20.1 ± 3.4		0.3 ± 0.1		
	CMT.9.A	+	+	+	Clade 1b	downstream	+	–	+	+	89.1 ± 1.6		27.5 ± 2.7		16.1 ± 1.4		
PNA	AN10	+	+	+	Clade 1a	downstream	–	clade II	+	+	62.2 ± 4.8	b	25.6 ± 5.0	abc	24.9 ± 1.8	ab	
	19SMN4	+	+	+	Clade 1a	downstream	–	–	+	+	44.0 ± 2.5		29.3 ± 1.7		25.6 ± 3.0		
	CCUG 11256	+	+	+	Clade 1a	downstream	–	–	+	+	43.7 ± 3.3		20.4 ± 1.6		18.0 ± 1.2		
LNA	DNSP21	+	–	–	Clade 1a	downstream	–	–	+	+	1.2 ± 0.01	c	9.1 ± 0.6	abc	6.5 ± 0.3	bc	
	24a75	+	+	–	Clade 1a	downstream	–	–	+	+	11.3 ± 0.7		47.4 ± 4.3		83.7 ± 44.6		
	DSM 50238	+	+	–	Clade 1a	downstream	–	–	+	+	0.01 ± 0.01		13.9 ± 0.7		56.9 ± 13.6		
	DSM 18231	+	+	–	Clade 1a	upstream	–	clade I	+	+	0.2 ± 0.07		43.1 ± 4.2		21.4 ± 5.6		
	4C29	+	+	–	Clade 1a	upstream	–	–	+	+	17.1 ± 6.7		41.2 ± 3.0		88.9 ± 26.5		
	28a3	+	–	–	Clade 1a	upstream	–	–	+	+	1.38 ± 0.01		28.4 ± 8.5		52.6 ± 27.5		
	JM300	+	+	–	Clade 1b	upstream	+	clade I	+	+	1.6 ± 0.04		38.6 ± 13.8		67.0 ± 25.7		

Table 1. Denitrification-related genetic features and maximum accumulation of the intermediate products of 18 *Stutzerimonas* strains. The strains were characterized and grouped as full nitrite accumulators (FNA), partial nitrite accumulators (PNA) or low nitrite accumulators (LNA). The two nitrite reductases NirS and NirK were classified into different clades according to Jones et al. (2008). The genetic organization of the *nirS* related clusters *nirMCFDLGH*, located directly downstream and *nirQOP,* positioned directly upstream of *nirS*, was the same in all strains. These are therefore not mentioned in the table. The *nirJENY* cluster was found either upstream or downstream of *nirS*, depending on the strain. All *nirK* clade I genes were accompanied by the accessory gene *nirV*, located directly downstream of the *nirK* gene, while all *nirK* clade II genes were followed by an extra *norCBQD* gene cluster, not shown in the table. Statistical significance for the maximum denitrification intermediates accumulation was assessed using one-way ANOVAs (p = 0.05). Post hoc multiple comparisons of means were conducted using Tukey´s Honest Significant Difference (HSD; p = 0.05) tests. Statistical differences are indicated where the groups sharing the same letter are not statistically different.